Procedia Manufacturing

Volume 5, 2016, Pages 828–837

44th Proceedings of the North American Manufacturing Research Institution of SME http://www.sme.org/namrc

# Investigation of Thickness Variation in Single Point Incremental Forming

Erika Salem[1a], Jaekwang Shin[1b], Maya Nath[1a], Mihaela Banu[1b*], Alan I. Taub[1a,b]

[1a]*Department of Materials Science and Engineering,*
[1b]*Department of Mechanical Engineering*
*University of Michigan, Ann Arbor, Michigan, U.S.A.*

erikasal@umich.edu, jkshin@umich.edu, nathm@umich.edu, mbanu@umich.edu, alantaub@umich.edu

**Abstract**
Incremental forming has great potential in manufacturing low volume, complex shapes. The process results in high local strains that are applied to the metal sheet, often exceeding the conventional formability limit. This paper is focused on investigating the influence of the tool strain path on formability and localized thinning of AA7075-O sheets in single point incremental forming. Through numerical models and experiments, the influence of the tool path on the cumulative strain along the wall of the formed sheet is established with consequences on dimensional accuracy.

*Keywords:* Single point incremental forming, Modeling and experimental investigation, Thickness variation

## 1 Introduction

Incremental Forming is a low tooling cost process with high potential to replace conventional deep drawing processes in customized manufacturing of complex components, e.g. aerospace applications and rapid prototyping for other industrial sectors. Initially, incremental forming was developed as Single Point Incremental Forming (SPIF) and later extended to Double Sided Incremental Forming (DSIF) (Malhotra, 2011) and Two Point Incremental Forming (TPIF) (Matsubara, 2001), (Ren, 2010). In its simplest form, these processes are highly flexible and can be implemented using existing equipment such as robots and CNC machines. In addition, the material formability is enhanced compared with conventional sheet metal forming processes, enabling forming of a wide range of

* Corresponding author

 Selection and peer-review under responsibility of the Scientific Programme Committee of NAMRI/SME


doi:10.1016/j.promfg.2016.08.068

angles, sharp radii and geometric asymmetries (Jeswiet, 2005). However, the parts formed by the current incremental forming processes can exhibit excessive thinning, springback and a lower surface quality compared with conventional forming processes. In addition, optimization procedures are not generally available for the incremental forming processes (Fratini, 2004).

A number of studies concluded that through-the-thickness shear and local bending of the sheet around the tool are the contributing factors in the SPIF fracture process (Martins, 2008), (Malhotra, 2012), (Silva, 2013). Local deformation of the sheet under the tool is composed of local stretching and bending. The accumulation of high plastic deformation in these areas can result in damage initiation. It is demonstrated through finite element methods (FEM) that this damage is not symmetric on the inner and outer faces of the sheet. This uneven distribution of damage explains the enhanced formability compared with conventional forming (Malhotra, 2012).

The stretching and bending of the metal sheet leads to a thinning of the walls according to the sine law (Henrard, 2011). To predict local thinning, Cao proposed an analytical algorithm for thickness calculations in multi-pass incremental forming based on rational Bezier curves (Cao, 2015). This algorithm predicts the thickness of cone-shape geometries, symmetric and non-axisymmetric. Other approaches for thinning prediction are based on stress-strain evaluation through a finite element analysis (FEA) (Neto, 2015). Neto showed that in SPIF, the deformation mode is close to a plain strain condition. Minor and major plastic deformation highlight the strain path which deviated towards biaxial stretching in the transition zone between the inclined wall and the bottom corner of the truncated cone (the cone shape proposed as benchmark at Numiform 2004). During modeling of SPIF, a negative mean stress was observed which they interpret as postponing ductile fracture by nucleation and growth of voids.

In SPIF, thinning of the sheets is a result of progressive loading, the accumulated strains and the uneven stresses generated by the contact with the tool. For some components, the variation of the thickness can negatively impact the functionality of the part in an assembly, when associated with local weakening of the mechanical properties. To address this issue, the present paper is focused on understanding the location of thinning along the walls in SPIF as well as the localization of the thinning in a specific area.

# 2 Experimental setup

To measure the deformation in SPIF, constant wall angle cones were formed from AA7075-O sheet metal. The plates were cut into 200 mm x 200 mm specimens and annealed from the as-received T6 condition into the O condition at $407^0$C for 2 hours. Once annealed, eight 6.35 mm holes were drilled into each sheet in an equally spaced circular pattern, and a grid composed of 2 mm diameter circles with center marks was electrochemically etched onto the back side of the sheet.

The experimental set up utilized is similar to that shown in Figure 1 (Martins, 2008). The blank is clamped between the blankholder and a backing plate, which each have a 160 mm circular opening. The blankholder is held against the backing plate with eight 6.35 mm bolts. This assembly is then clamped into the spindle chuck.

## 2.1 Process parameters

The tests were run on a Standard Modern 1700 Series CNC lathe and the spiral tool path was programmed using G-code. The starting point of the tool path was located close to the clamped edge of the sheet and the tool progressed from out-to-in (Figure 2).

The following settings were used:

- Forming angle = 67 degrees;
- Sheet thickness = 1.6 mm;
- Spindle speed = 5 rotations/minute;
- Step size = 0.5 mm/rotation

Five truncated cones were formed with an initial diameter of 140 mm and final depths of 20 mm, 30 mm, 35 mm, 45 mm and 55 mm. The forming tool is a rigid finger type tool with a 12.7 mm diameter hemispherical tip. To minimize friction, a commercial $MoS_2$ grease lubricant was applied continuously throughout the process.

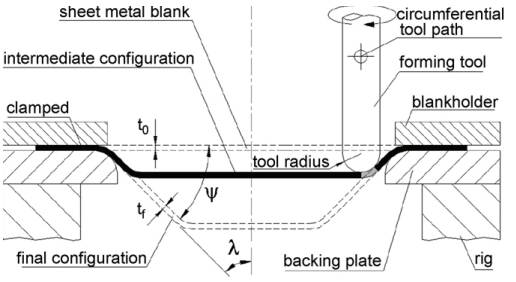


Figure 1 Experimental setup of SPIF on a lathe
(Martins, 2008)

## 2.2 Analysis methods

Three specimens 90 degrees apart were cut out from the wall of each cone. The edge of each specimen was polished to allow measurement of the local sheet thickness using optical imaging. The thickness profile of each section was determined using Image J software with a spacing of 0.25 mm between each point and confirmed at several points with a digital caliper. The thickness profile for each sample was normalized to the thickness of the original sheet held in the binder to eliminate any variance from camera height between images.

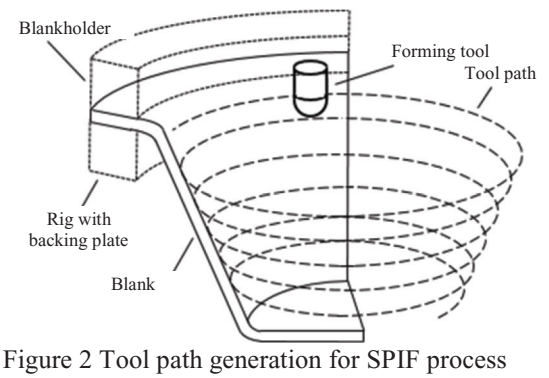


Figure 2 Tool path generation for SPIF process

# 3 Modeling setup of incremental forming

A finite element model of the SPIF process was created in ABAQUS dynamic explicit scheme. This finite element model was used to calculate the evolution of the stress and strain in the metal sheet during forming along the wall of the formed part. Dynamic explicit scheme was used in order to improve the convergence of the problem. The computation was done on Intel® Core™ i7–2600 K 40-Core processors. Five models were created with forming depths equal to the experimental cones. For each model, springback was calculated by unloading the tool and cancelling the non-equilibrated forces.

## 3.1 Model set-up

The metal sheet was meshed with a non-uniform mesh size optimized so that the areas with large deformation have a finer mesh. Three layers of elements were setup across the thickness. The mesh is shown in Figures 3a,b. The metal sheet was clamped between two plates, upper blankholder and lower blankholder. The blankholders are rigid bodies and meshed with R3D4 elements (Dassault Systems, 2011). The dimension of the square blank is 208 mm at its edges, with a thickness of 1.6 mm. To accurately calculate the geometry resulting from the spiral tool path, a circumferential mesh is applied.

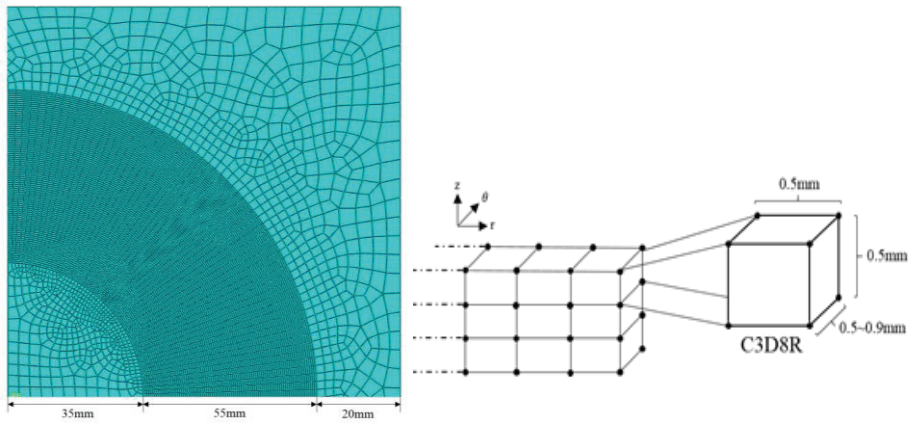


a) b)

Figure 3 Mesh size and distribution in the blank; a) mesh distribution in the blank, coarse mesh size and fine mesh size, b) finite element distribution across the thickness

The distribution of the elements is: 60 elements in the circumferential direction with 0.5 mm length and thickness every 90° resulting in a total of 240 elements in the circumference and 3 layers in the thickness direction. The tool has the radius of 6.35 mm and was meshed with a rigid element of size of 0.4 mm to give sufficient resolution between the tool and blank interface. The blankholder has the same outer dimension as the blank and the inner diameter of 160 mm was also meshed with rigid elements.

The blankholder force is applied through a coupling of continuum distributing method (Dassault Systems, 2011). A large force (1000kN) was applied to the central point using this method, so that no material flow would occur between the blankholders.

## 3.2 Constitutive material model

We used the material properties for AA7075-O determined by tensile testing. The measured Young's modulus of 72 MPa matches reported data (ASM International, 1990). The material was assumed to be elasto-plastic isotropic and an isotropic hardening rule was assigned. The stress strain data was introduced as raw table data. The Poisson's ratio was assumed to be 0.33 (ASM International, 1990). No boundary condition had been imposed on the blank, which is held in place by the blankholder and the backing plate of the rig, with the blankholder applying downward vertical force. The forming tool path was the same as the one programmed in the experimental setup, and was implemented in the model through an external subroutine.

General Contact algorithm provided by ABAQUS was used to specify the contact (Dassault Systems, 2011). The general contact algorithm allows for independent specification of the interaction domain, contact properties and surface attributes but also acts more robustly than its traditional counterpart, which requires assignment of all slave and master surfaces. Two contact properties, tangential and normal, behavior, were specified between the forming tool and blank, blankholder and the blank, and the blank and backing plate. The tangential behavior used was a classical isotropic Coulomb friction model, which allows the friction coefficient to be defined in terms of slip rate, contact pressure and average surface temperature at the contact point. We have specified a friction coefficient of 0.15 which is consistent with other studies (Eyckens, 2010). The normal behavior specifies a hard contact relationship, which minimizes the penetration of the slave surface into the master surface at the constraint locations. It does not allow for the transfer of tensile stress across the contact interface.

## 3.3. Simulation of SPIF

Five models were simulated in order to obtain truncated cones with 20 mm, 30 mm, 35 mm, 45 mm and 55 mm depth. For 55 mm depth, the total computation time of the simulation was 636 seconds using a standard time increment in ABAQUS. The dynamic explicit scheme was used with a mass scaling factor $10^7$. This value was determined by trial and error so that the ratio between kinetic energy and internal energy to remain below 5%.The output of this simulation was set to illustrate the distribution of equivalent stress, equivalent plastic strain, displacements and energy. The energy was used in calculation of the ratio between the kinetic energy and internal energy, an indicator of steady-state dynamic calculations. Among the sets of output, equivalent plastic strain and displacements were used for analyzing the thinning of the sheet. Five samples were virtually cut from the formed cones (Figure 4).

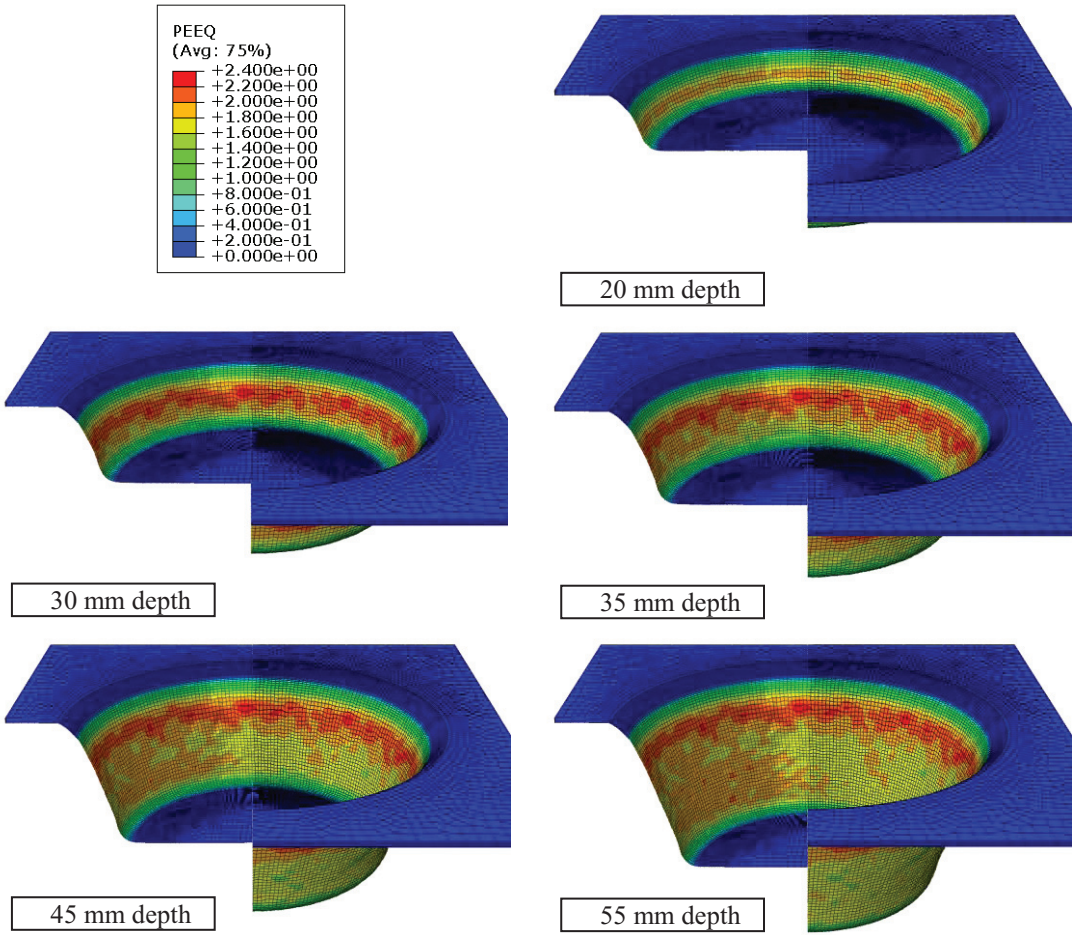


Figure 4 Distribution of the equivalent plastic deformation at forming the truncated cone

# 4 Results and discussions

Figure 5 shows a photo of one of the experimental specimens and the corresponding thickness profile. Three distinct regions are seen. Near the blankholder, we observed a region with a bent shape and a continuous thickness reduction. Below that, we observed a section with pronounced thinning compared with the steady state thickness region.

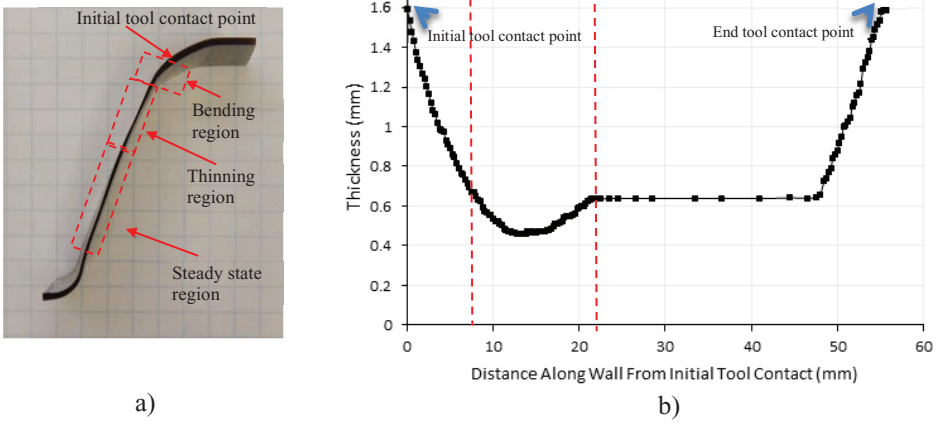


Figure 5 Thickness variation measured on the samples; a) example of a sample cut from the truncated cone of 55 mm depth, b) thickness variation along the wall from the initial contact

## 4.1. Model evaluation of the thinning

To compare the model and experimental results, strips were virtually cut from the formed cone models after springback, corresponding to the five formed depths: 20 mm, 30 mm, 35 mm, 45 mm and 55 mm. Thickness was calculated through the difference between the coordinates of the nodes from the inner layer and outer layer. Due to large deformations accumulated in the sheet, some of the finite elements exhibited rotations. An algorithm to calculate the actual thickness of the formed sheet was created and implemented in MATLAB. The algorithm is schematically represented in Figure 6 and depicted in eq. (1-6).

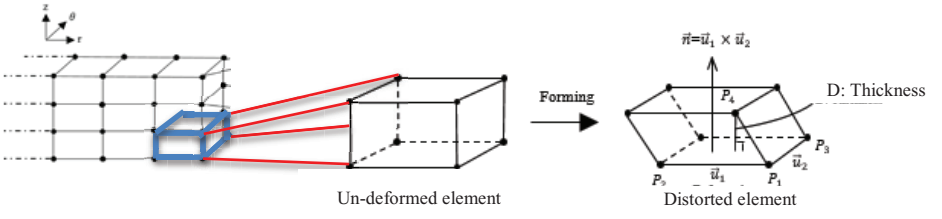


Figure 6 Calculation of the thickness after deformation (D)

$$P_i = (x_i, y_i, z_i), i = 1,2,3 \quad (1)$$
$$\vec{u}_1 = P_{i+1} - P_i \quad (2)$$
$$\vec{u}_2 = P_{i+2} - P_i \quad (3)$$

$$\vec{n} = \vec{u}_1 \times \vec{u}_2 \quad (4)$$

The equation of plane in $R^3$ is $ax + by + cz + d = 0$, where $\vec{n} = (a, b, c)$,

$$a = \vec{n} \cdot (1,0,0), \mathrm{b} = \vec{n} \cdot (0,1,0), \mathrm{c} = \vec{n} \cdot (0,0,1), \mathrm{d} = \vec{n} \cdot (0,0,0) \quad (5)$$

$$D = \frac{|ax_3 + by_3 + cz_3 + d|}{\sqrt{a^2 + b^2 + c^2}} \quad (6)$$

The comparison between thinning of the sheet in simulation and experiments was done for a specific area of the cut strips with focus on the most critical areas. To cancel the numerical instabilities caused by a reduced number of nodes, a fitting curve was used for the simulation set of data.

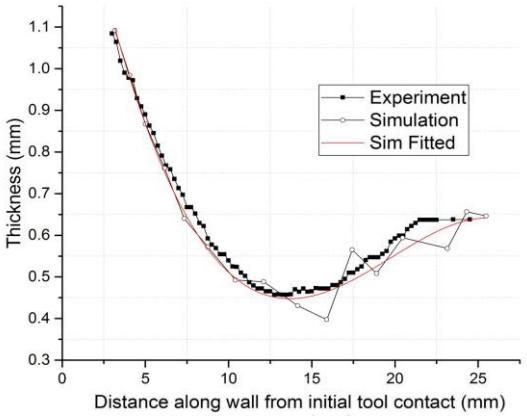


Figure 7 Comparison between simulation and experimental results of thickness evaluation in the thinning area

The thickness, D, is averaged over the three elements across the sheet. The model shows very good agreement of the thinning observed in the experimental samples (Figure 7). Moreover, the position of the maximum thinning along the wall is predicted very well.

## 4.2. Thinning localization depending on the tool path

To plot the accumulated plastic strain in the bending, thinning and steady state regions, three series of monitoring elements were created in ABAQUS. These elements were selected to be the most representative in showing the accumulated strains. Thus, the element labels of a column of these elements from the thickness were identified. With the label of these elements, three series of monitoring areas were created: Series A, Series B and Series C, corresponding to bending, thinning and steady state regions, respectively (Figure 8). A new simulation was run up to 55 mm depth recording the equivalent plastic strain for the three selected series.

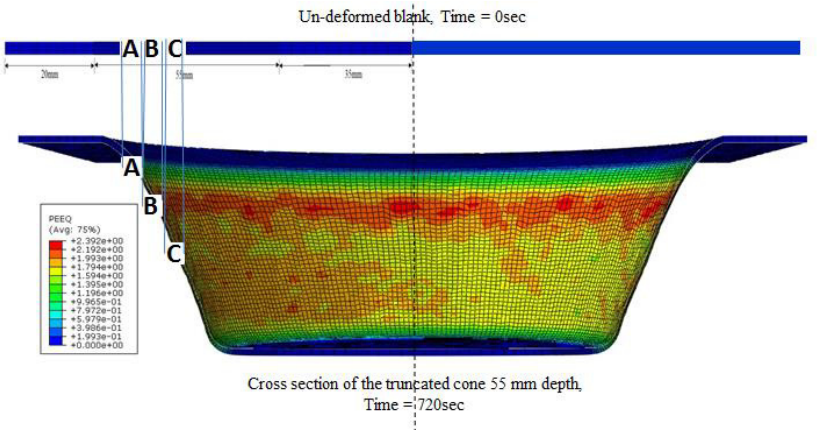


Figure 8 Equivalent plastic strain history for thinning area along the wall. Identification of the Series A, B and C on the formed cone

The simulation shows that in all three regions, there is limited strain and thinning prior to and following the tool contact. This confirms that the deformation in SPIF is dominated by localized plastic deformation under the tool. The grey bar in Figure 9 indicates the point in time when the tool is in contact with the element of interest belonging to each series A, B and C.

Further analysis is underway to determine the mechanism that initiates the excessive thinning region that develops after the bend region and the start of the steady state region.

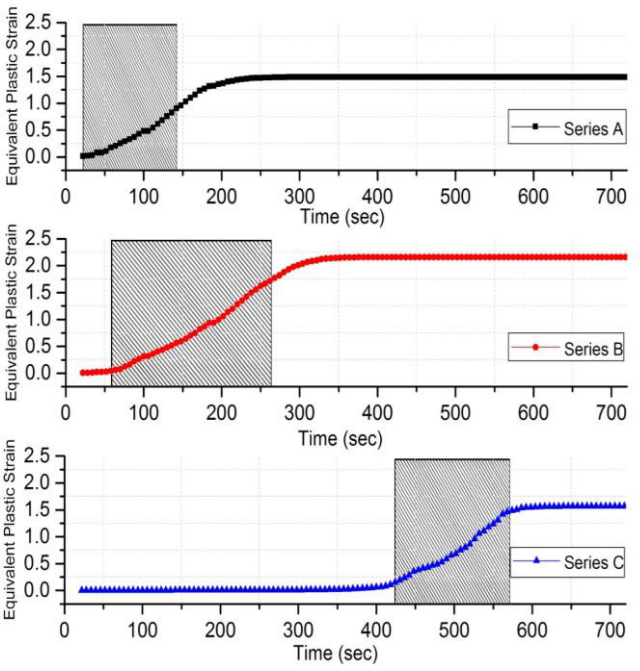


Figure 9 Equivalent plastic strain of the wall at various forming tool passage. The left edge of the grey bar signifies the leading edge of the tool contact and the right edge signifies the trailing edge of the tool contact

# 5 Conclusions

SPIF process was applied to perform five truncated cones with progressive depths: 20 mm, 30mm, 35 mm, 40mm and 55mm.

Thickness variation along the wall of the cones was analyzed through measurements. The measurements revealed three distinct regions on the wall: bending, thinning and steady

state. A finite element model was created and experimentally validated. Further, the model was used to understand the evolution of the nature of the thinning area, location of thinning and its size.

Modeling the evolution of the thickness reduction indicates that the majority of the thinning occurs under the tool. Modeling without a damage criterion was able to accurately predict thinning during SPIF of a truncated cone. At the start of the cone forming, a bending region is seen with continuous thickness reduction. Then a region of excessive thinning develops, followed by a steady state region with constant thickness.

# References

Badr, M. O, Rolfe, B., Hodgson P., Weiss, M., The numerical investigation of the material behavior of high strength sheet materials in incremental forming, *AIP Conference Proceedings 1532*, 513, 2013.

Cao T., Lu B., Xu D., Zhang H., Chen J., Long H., Cao J., An efficient method for thickness prediction in multi-pass incremental sheet forming, *The International Journal of Advanced Manufacturing Technology* (77) 469-483, 2015.

De Sena, J. I.V., Guzmán, C. F., Duchêne, L., Habraken, A. M., Behera, A.K., Duflou, J., Valente A. F., Sousa, R. J., Simulation of a Two-Slope Pyramid Made by SPIF using an Adaptive Remeshing Method with Solid-Shell Finite Element, *International Journal of Material Forming*, p. 1-12, DOI 10.1007/s12289-014-1213-8, 2015.

Fratini,L., Ambrogio, G., Di Lorenzo, R., Filice, L., Micari, F., Influence of mechanical properties of the sheet material on formability in single point incremental forming, *CIRP Annals - Manufacturing Technology*, Volume 53, Issue 1, Pages 207-210, 2004.

Governale, A., Lo Franco, A., Panzeca, A., Fratini, L., Micari, F., Incremental Forming Process for the Accomplishment of Automotive Details, *Key Engineering Materials*, 344, 559-566, 2007.

Henrard, C., Bouffioux C., Eyckens, P., Sol. H., Duflou J.R., Van Houtte P., Van Bael, A., Duchene, L., Habraken, A.M., Forming forces in single point incremental forming: prediction by finite element simulations, validation and sensitivity, *Computation Mechanics* 47:573-59, 2011.

Huang, Y., Wang, Y.J., Cao, J., Li, M., Prediction of Forming Limit in Single Point Incremental Forming with the Ductile Fracture Criterion, *Proceedings of the 2007 International Manufacturing Science And Engineering Conference, MSEC2007*, Oct.15-17, 2007, Atlanta, Georgia, USA.

Jeswiet, J., Micari, F., Hirt, G., Bramley, A., Duflou, J., Allwoo, J., Asymmetric Single Point Incremental Forming of Sheet Metal, *CIRP Annals - Manufacturing Technology*, 54 (2): 88 -114, 2005.

Lu, B., Fang, Y., Xu, D., and Chen, J., An analytical approach for investigation of the incremental sheet forming process, *AIP Conference Proceedings 1567*, 868, 2013.

Maier, C., Failure prediction in sheet metal forming using FEA of Nakazima test, *Machines, Technologies, Materials*, ISSN 1313-0226, 7, 1-12, 2013.

Malhotra R., Xue L., Belytschko T., Cao J, Mechanics of fracture in single point incremental forming, *Journal of Materials Processing Technology*, 212, 1573-1590, 2012.

Martins, P.A.F., Bay, N., M. Skjoedt, Silva, M.B., Theory of single point incremental forming, *CIRP Annals - Manufacturing Technology*, 57, 247-252, 2008.

Matsubara S., A Computer Numerically Controlled Dieless Incremental Forming of a Sheet Metal, *Journal of Engineering Manufacturing*, 215, 959-966, 2001.

Dassault Systems, (2011), *ABAQUS Analysis User's Manual* (v.6.11), Providence, RI, USA.

Dassault Systems, (2011), *ABAQUS Theory Manual* (v.6.11), Providence, RI, USA.

Neagoe I., Filip A.C., Vasiloni M.A., Experimental Researches on the Limit Angle of Conical Parts Manufactured by Single Stage Incremental Forming on CNC Lathes, *Applied Mechanics and Materials* (371):168-172, 2013.

Neto D.M., Martins J. M. P., Oliveira, M. C., Menezes, L.F., Alves, J.L., Evaluation of strain and stress states in the single point incremental forming process, *The International Journal of Advanced Manufacturing Technology*, 1-14, 2015.

Ren F., Cui Z., Xia C., Slavik, T., Zhang, L., Zhu X., *Process Modeling of Freeform Incremental Forming using LS-DYNA*, 11th International LS-DYNA Users Conference: 10-1-10-6, 2010.

Skjoedt, M., Silva, M.B., Martins, P.A.F., Bay, N., Strain Paths and Fracture in Multi Stage Single Point Incremental Forming, *The 9th International Conference on Technology of Plasticity*, Gyeongju, Korea, 2008.

Silva, M.B., Martins, P.A.F., Two-Point Incremental Forming with Partial Die: Theory and Experimentation, *Journal of Materials Engineering and Performance*, 22(4): 1018-1027, 2013.

Van Bael A., Eyckens, P., He S., Bouffioux, C., Henrard C., Habraken A.M., Duflou J., Van Houtte P., Forming Limit Predictions for Single-Point Incremental Sheet Metal Forming, *Proceedings of ESAFORM Conference on Material Forming*, 309-314, 2007.

Voswinckel H., Bambach M., Gerhard Hirt G., Improving geometrical accuracy for flanging by incremental sheet metal forming, *International Journal of Material Forming*, 8: 391–399, 2015.

ASM International, *Properties of Wrought Aluminum and Aluminum Alloys, Properties and Selection: Nonferrous Alloys and Special Purpose Materials*, (2): 62-122, 1990.